ACS OMEGA

Open Access

http://pubs.acs.org/journal/acsodf

Article

Analysis of Near-Wall Pebble Bed Thermal Conductivity for Energy Applications

Katelyn Wada, Josh Eixenberger, Dallin Stout, Brian J. Jaques, Todd Otanicar, and David Estrada*

Cite This: *ACS Omega* 2024, 9, 1614−1619

Read Online

ACCESS | Metrics & More | Article Recommendations

ABSTRACT: Pebble beds have been employed in thermal storage and energy systems, where they are typically used to promote heat exchange in high-temperature environments. Understanding the heat conduction of the entire pebble bed could aid in the material selection of the pebbles themselves and structural components, system design, and safety monitoring. However, the thermal conductivity of pebble beds can change significantly near geometric boundaries. Using a complex multilayer analytical model in conjunction with a line source probe, we found a substantial increase in the thermal conductivity of a sintered bauxite pebble bed in the near-wall region (7.6 W m^{-1} K^{-1}) compared to the bulk (0.59 W m^{-1} K^{-1}). We investigated this difference by comparing porosity results, acquired with micro-CT, of 33.18 and 33.31% at approximately one pebble width surrounding the probe (near-wall) and the bulk of the pebble bed, suggesting that the thermal conductivity is largely altered by thermal contact resistance in the near-wall regime.

INTRODUCTION

Pebble beds have gained considerable traction in recent years for thermal storage and energy systems (Figure 1).[1] A breadth of benefits can be gained by using solid pebble beds for photovoltaics, wind energy, and nuclear energy storage systems, including reduced cost, increased safety, and operable working temperatures compared to liquid heat storage systems.[2−4] In addition, advanced next-generation pebble bed reactors (PBRs) have been highly rated for their safety and thermal efficiencies.[5−7] PBRs provide the option of being gas-cooled or molten salt-cooled, which can further increase their performance.[6,8] Pebble bed scenarios are also important for geothermal applications where discerning thermal properties is critical for efficiency in energy conversion, sustainability, environmental impact, economic viability, and structural performance.[9,10] In any case, developing models and measurement techniques for thermal properties and accurately depicting thermal transport in these pebble beds is crucial for their continued advancement (Table 1).

Previous efforts have been made to model the extremely complex geometry of pebble bed systems, which are typically accompanied by computationally difficult random and repeated unit cell simulations.[11−16] Most studies have gathered temperature profiles and thermal conductivities across the entire sample range into a lumped thermal result. However, variations in the thermal conductivity at geometric boundaries are inevitable.[17−19] The packing and porosity of the pebbles largely dictate the rate of heat conduction.[20] Some studies have demonstrated modeling and experimental results comparing "near-wall" effects with the bulk, taking "near-wall" to be both hot and cold sides of a (typically) rectangular shape.[17−19] Results have shown that the "near-wall" region, which has higher porosity, demonstrates a lower thermal conductivity than the bulk.

Having a low thermal conductivity at boundaries can lead to localized overheating, potentially causing instrumental or structural damage. Understanding this behavior is paramount for safety considerations and material selection processes. Here, we highlight a novel layered analytical model and measurement technique for thermal conductivity determination of a pebble bed and relate the results to porosity in the bulk and near-wall regimes acquired via micro-CT.

METHODS

A sintered bauxite pebble bed sample passing the no. 40 sieve (425 μm) and retained on the no. 70 (212 μm) sieve (40/70) was chosen for measurements (Figure 2). Sintered bauxite has been a promising material utilized in energy storage and thermal transport systems and presents a wide working temperature window (673−1273 K).[2,12,21−23] We used our previously developed line source method[24,25] to elucidate the thermal conductivity of the sintered bauxite pebble bed sample. This technique has been shown to enhance the capabilities of the traditional line heat source technique for thermal conductivity measurements of solid samples acting as surrogate nuclear fuels.[26−32] Here, we present the technique as a promising approach for determining the thermal conductivity near the inner wall (Figure 3a) of a pebble bed system compared to the thermal conductivity deeper into the bulk of the material.

Received: October 18, 2023
Revised: December 7, 2023
Accepted: December 13, 2023
Published: December 28, 2023

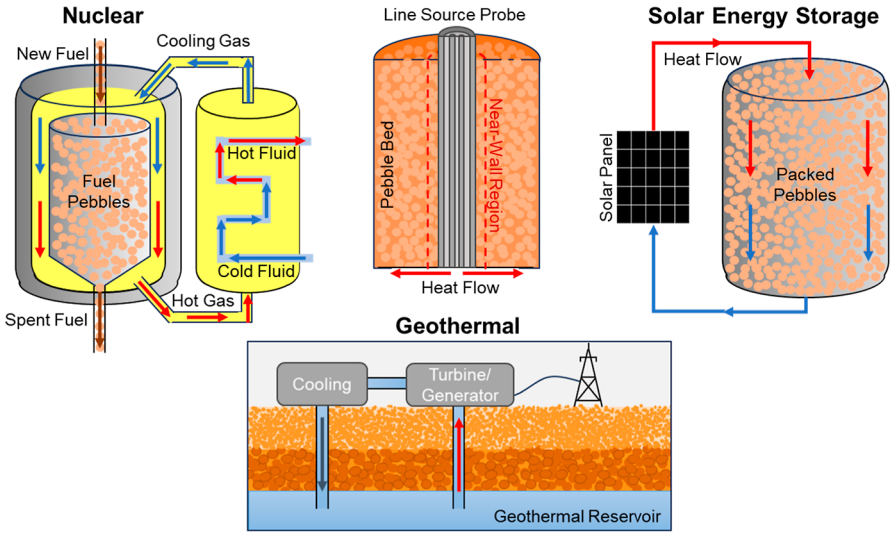

Figure 1. Applications for pebble bed thermal property measurements using a line source probe.

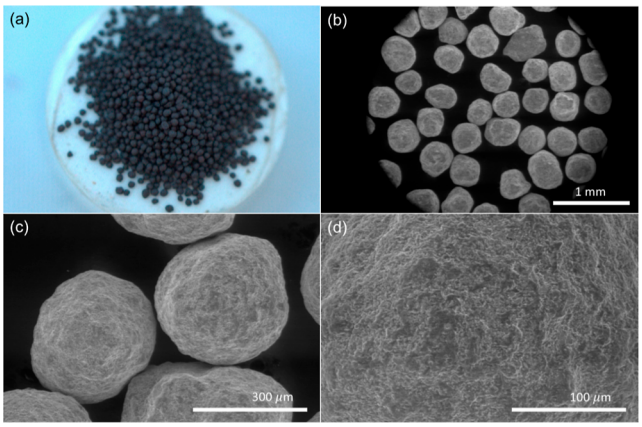

Figure 2. (a) Optical image of 40/70 sintered bauxite pebbles and (b,d) SEM images of sintered bauxite pebbles at various magnifications.

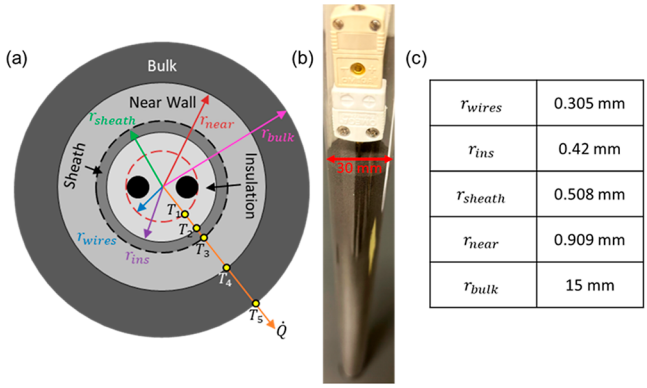

r_{wires}	0.305 mm
r_{ins}	0.42 mm
r_{sheath}	0.508 mm
r_{near}	0.909 mm
r_{bulk}	15 mm

Figure 3. (a) Cross-sectional geometry of the probe in the pebble bed. (b) Image of the probe inserted in the 30 mm diameter pebble bed. Here, r_{sheath} is the sheath radius, r_{wires} is the radius of the effective wire layer, $r_{insulation}$ is the insulation radius, r_{near} is the near-wall radius, r_{bulk} is the bulk sample radius, $\dot{Q}$ is heat flux, and T_1, T_2, T_3, and T_4 are temperature solutions at the layer boundaries, and (c) table containing the numerical values for the radii of each layer.

The sintered bauxite pebble bed was measured in a cylindrical tube 30 mm in diameter. A 1 mm diameter Type-k thermocouple probe, utilizing the thermocouple wires as a heating element, was inserted into the centerline of the pebbles for measurements of the system (Figure 3b). The measured temperature profile was then fitted to a multilayered analytical model with the bulk thermal conductivity set to 0.22 W m^{-1} K^{-1} as found through a plane source probe technique, which is comparable to literature values of 0.23 W m^{-1} K^{-1}.[33] The bulk thermal diffusivity was set to 0.15 mm^2 s^{-1} to allow extraction of the near-wall thermal properties. Thermal diffusivity values of 40/70 sintered bauxite are lacking in the literature; however, a pellet of sintered bauxite has been reported to have a thermal diffusivity of 2.8 mm^2 s^{-1} at room temperature and a thermal conductivity of 6.5 W m^{-1} K^{-1} which would correlate to the thermal property values of a solid sintered bauxite.[33]

A DC current was used to induce Joule heating in the probe, while a small AC signal was superimposed to obtain temperature-dependent voltage measurements with a lock-in amplifier. After conversion of the voltage measurement to temperature, the temperature profile can be compared to an analytical model to extract the thermal conductivity. The thermal quadrupoles approach[34] was utilized to generate a multilayered analytical model to extract the thermal conductivity of the various layers, including the near-wall layer. In this case, we have selected two near-wall regions, both immediately surrounding the probe, one that is approximately 0.4 mm thick in addition to a smaller selected region of 0.14 mm thick. A simplified effective 1-wire geometry[25] is modeled as eq 1 (with coefficients in Table 1), and fit to the experimental measurements with a two-parameter fit varying thermal conductivity and diffusivity of the near-wall layer.

$$\begin{bmatrix}\theta_1\\ \varphi_1\end{bmatrix} = \begin{bmatrix}A_1 & B_1\\ C_1 & D_1\end{bmatrix}\begin{bmatrix}1 & 0R_{th,1}\\ 0 & 1\end{bmatrix}\begin{bmatrix}A_2 & B_2\\ C_2 & D_2\end{bmatrix}\begin{bmatrix}A_3 & B_3\\ C_3 & D_3\end{bmatrix}\begin{bmatrix}1 & 0R_{th,2}\\ 0 & 1\end{bmatrix}\begin{bmatrix}A_4 & B_4\\ C_4 & D_4\end{bmatrix}\begin{bmatrix}A_5 & B_5\\ C_5 & D_5\end{bmatrix}\begin{bmatrix}1 & 0\\ h & 1\end{bmatrix}\begin{bmatrix}\theta_3\\ \varphi_3\end{bmatrix} \quad (1)$$

where θ is the Laplace temperature, φ is the Laplace heat flux, R_{th} is thermal contact resistance, h is the convection coefficient, index 1 corresponds to the effective wire layer, index 2 is the insulator layer, index 3 is the sheath layer, index 4 is the near-wall layer 0.4 mm thick, and index 5 is the bulk sample. In this

https://doi.org/10.1021/acsomega.3c08202
ACS Omega 2024, 9, 1614−1619

Table 1. Coefficients for the Material Matrices in eq 1[a]

insulation, sheath, and sample layers	effective wire layer
$q_{1,i} = r_i\sqrt{\frac{p}{\alpha_i}}, q_{2,i+1} = r_{i+1}\sqrt{\frac{p}{\alpha_i}}$	$q_i = r_i\sqrt{p/\alpha_i}$
$A_i = q_{2,i}\,[I_0(q_{1,i})K_1(q_{2,i}) + I_1(q_{2,i})K_0(q_{1,i})]$	$A_i = 1$
$\mathrm{Bi} = 1/2\pi\mathrm{kL}[I_0(q_{2,i})K_0(q_{1,i}) - I_0(q_{1,i})K_0(q_{2,i})$	$B_i = 1/2\pi kLI_0(qi)/q_iI_1(q_i) - 1/\rho c\pi r_i^2 Lp$
$C_i = 2\pi kLq_{1,i}\,q_{2,i}[I_1 - (q_{2,i})K_1(q_{1,i}) - I_1(q_{1,i})K_1\,(q_{2,i})]$	$C_i = \rho c\pi r_i^2\,Lp$
$D_i = q_{1,i}\,[I_0(q_{2,i})K_1(q_{1,i}) + I_1(q_{1,i})K_0(q_{2,i})$	$Di = q_i2I_0(q_i)/2I_1(q_i)$

[a] α = thermal diffusivity, p = Laplace parameter, r = radius, k = thermal conductivity, L = length, I and K = modified Bessel functions, ρ = density, and c = specific heat capacity.

instance, h has a negligible effect on the temperature profile since the bulk section of pebbles is large enough, with respect to the amount of heating and time range of the measurements, and since the pebbles are held in a plastic tube.

The porosity of the bulk and near-wall layers was obtained from micro-CT scans of the probe in the sample. From the micro-CT scan, the sample was segmented into four different regions by defining the different regions of interest and segmenting the pebbles from the probe using the differences in optical density: a bulk segment of pebble beds without the probe, the probe itself (Figure 4a), a near-wall segment (Figure 4b,d,e) approximately the width of a single pebble (0.4 mm), and the probe and near-wall segment approximately half the width of a single pebble (0.14 mm) shown in Figure 4c. Since the selected regions of interest included the pebbles and probe, and the optical density range selected included the pebbles and the insulation of the probe, it was necessary to remove the insulation's contribution to the porosity of the probe and near-wall segments. The object volume from the insulation segment was subtracted from the probe and near-wall segments to obtain the object volume for the pebbles in the near-wall layer.

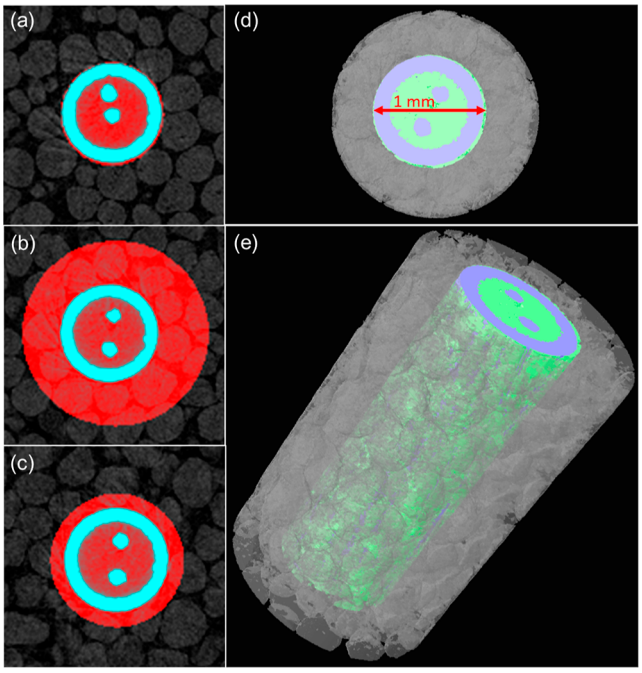

Figure 4. Micro-CT images of (a) probe region of interest (ROI) highlighted (red) inside the pebble bed, (b) area of the 0.4 mm near wall around the probe, (c) area of the 0.14 mm near wall around the probe, (d) 1 mm diameter probe and surrounding near-wall section, and (e) length view of the volume selected for the near-wall scan.

The total volume of the insulation segment, which accounts for the full volume of the cylinder created from the probe, was subtracted from the total volume of the probe and near-wall segments to achieve the total volume of just the pebbles in either of the near-wall calculations. The object volume divided by the total volume will thus yield the percent of objects in the volume, and subtracting this value from 100% gives the porosity.

RESULTS AND DISCUSSION

A model removing the near-wall layer and modeling the entire sample as a single layer has been constructed as a comparison (Figure 5a). The effective thermal conductivity and diffusivity values achieved through a two-parameter fit were 0.59 W m^{-1} K^{-1} and 0.13 mm^2 s^{-1}, with a thermal contact resistance between the sheath and sample of 1 Km^2 W^{-1} and a coefficient of determination (R^2) value of 0.99. The thermal diffusivity here is comparable to the value of 0.15 mm^2 s^{-1} achieved through the plane source technique. However, the thermal conductivity value is twice the value bulk pebble beds should have.[35] Here, we speculate that the near wall is affecting the thermal conductivity value achieved. With the addition of the near-wall layer, which is 0.4 mm thick (Figure 5b), the temperature profiles match well between the experimental and analytical modeling results by setting the bulk thermal properties to values obtained through the plane source technique (0.22 W m^{-1} K^{-1} and 0.15 mm^2 s^{-1} for thermal conductivity and diffusivity) and varying the thermal conductivity and diffusivity of the near-wall layer. Increasing the thermal contact resistance to 2.5 Km^2 W^{-1} was necessary to achieve an appropriate shape to fit the experimental data. The thermal conductivity and diffusivity values of the near wall were found to be 7.6 W m^{-1} K^{-1} and 0.14 mm^2 s^{-1} with an R^2 value of 0.99. A model regarding the smaller 0.14 mm thick was constructed; however, setting the bulk properties to their smaller values obtained through the plane source technique would force the effective thermal conductivity of the 0.14 mm thick near-wall layer to increase substantially, which is not necessarily indicative of the thermal conductivity of that area but is a necessary effective compensation to ensure the model matches the measured results. This result suggests a gradient thermal conductivity that decreases radially outward, which has also been confirmed in the literature.[19]

A sensitivity parameter study (Figure 5c) was conducted to ensure the uniqueness of the near-wall solution. During the time range of the measurements (approximately 5−30 s), the sensitivity for the bulk thermal conductivity is significantly lower than for the 0.4 mm near-wall thermal conductivity. This study demonstrates that the properties of the near-wall layer, namely the thermal properties and radius, and the thermal contact resistance between the probe and sample are the

https://doi.org/10.1021/acsomega.3c08202
ACS Omega 2024, 9, 1614−1619

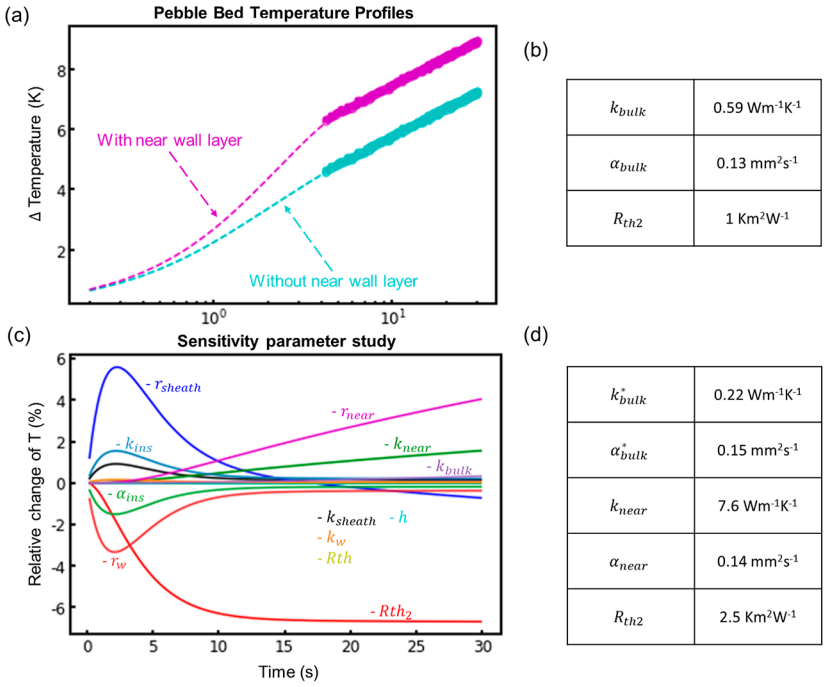

Figure 5. (a) Analytical modeling results for the pebble bed with and without a near-wall layer depicted with magenta and cyan dashed lines, respectively, with two experimental measurements as closed and open circles for each model, (b) table of values extracted from the analytical model of the bulk pebbles, (c) sensitivity parameter study of the analytical model with a near-wall layer, and (d) table of values extracted from the analytical model of the near-wall layer. Here, k, α, r, h, Rth, and Rth$_2$ indicate thermal conductivity, diffusivity, radius, convection coefficient, thermal contact resistance between wire and insulation, and thermal contact resistance between the sheath and sample, respectively. The subscripts w, ins, sheath, bulk, and near indicate the wire, insulation, sheath, bulk pebbles, and near-wall layers, and the superscript * indicates set values, respectively.

primary contributors to the temperature change in this time interval. The sensitivity parameter study shown in Figure 5c demonstrates that the near-wall thermal properties dominate the temperature distribution during the measurement time interval. The bulk properties start to show up near the end of the measurements (~30 s). These results indicate that the near-wall solutions are unique and identifiable compared to the bulk. The sensitivity parameter study shows that an optimal region of interest for discerning the thermal properties of the near-wall region is around 15−30 s.

As obtained from micro-CT, the bulk pebble bed had a porosity value of 33.31%, and the 0.4 mm near-wall segment had a slightly lower porosity of 33.18%. The 0.14 mm near-wall segment had a porosity of 61%, which is significantly higher. This value seems conceptually valid as there are only partial pebbles included since the width of the near wall is less than the diameter of a pebble. The spike in porosity at the edges of geometric boundaries has been previously reported in the literature.[19] This difference in porosity may explain the variation in the effective thermal conductivity of the pebble bed. The thermal conductivity of air (0.026 W m^{-1} K^{+36}) is much lower than the thermal conductivity of the pebbles. Having more space in between the pebbles and thus a higher porosity could contribute to a lower thermal conductivity. The difference in the porosity values, however, is not large enough to account for the large jump in thermal conductivity in the 0.4 mm near wall as compared to the bulk. According to Maxwell and Rayleigh's equation[37] (eq 2) relating the thermal conductivity of a composite k to its porosity P, and assuming the porosity is the only thing effecting the change in thermal conductivity, the thermal conductivity of the less porous near-wall region should only be about 0.3% higher than the thermal conductivity of the more porous bulk region. Here, subscripts s and g indicate solid and gas.

$$\frac{k}{k_s} = \frac{1 - \left(1 - \frac{3k_g}{2k_s + k_g}\right)P}{1 + \left(\frac{3k_s}{2k_s + k_g} - 1\right)P} \quad (2)$$

In addition, previous work has documented a proportional relationship between the thermal conductivity and temperature of sintered bauxite.[20] If the temperature difference between the center portion of the pebble bed closest to the heating element, the near-wall region, and farther away from the heating element, the bulk region, is large enough, there would in turn be a change in the thermal conductivity. However, a change of less than 9 K, as shown in Figure 5a, would have a nearly negligible effect on the thermal conductivity. Additionally, the thermal contact resistance has been shown to have an impact on the extracted effective thermal conductivity.[38] If the thermal contact resistance is higher than predicted, the resulting extracted thermal conductivity could be higher than its actual value. However, the thermal contact resistance and thermal conductivity affect the temperature profile differently, as shown by the sensitivity parameter study in Figure 5c. Changing the thermal contact resistance largely effects the magnitude and shape of the distribution, which alters the length and linearity of the region occupied by the experimental measurements, whereas changing the thermal conductivity largely effects the slope of the distribution. As such, these parameters can be uniquely identified. The porosity and temperature differences within the pebble bed have largely been debunked as the

https://doi.org/10.1021/acsomega.3c08202
ACS Omega 2024, 9, 1614−1619

culprits for the discrepancy in the thermal conductivity result in the near wall compared to bulk values, and the thermal contact resistance is not only used in the analytical model, which increases the validity but also is able to be uniquely distinguished from thermal conductivity, leading to a more accurate result.

However, since the width of the near-wall section analyzed is close to the diameter of a single pebble and measurements of a packed pellet of similar material[33] indicate that a single pebble has a thermal conductivity near 6.5 W m^{-1} K^{-1} it seems possible that the results of the near-wall region depict the thermal property values of the pebbles themselves or that the effective thermal conductivity of the pebble bed in this region reflects the thermal conductivity of a single pebble. To further understand the thermal physics in the near-wall regime, the material and size of the pebbles could be varied, as could the thermal conductivity and porosity measurements. Additionally, other gases or liquids with different thermal conductivities could be utilized to verify the results under different thermal fluid conditions.

In addition, error analysis was conducted to ascertain any uncertainty in the experimental measurements. The measurements of small electronics in the setup were conducted with a Keithley DMM6500 6 1/2 Digit Multimeter accurate up to 0.0001%, the SR865A 4 MHz DSP Lock-in Amplifier that measures the voltage that is converted to temperature is accurate up to 0.01%, and the SRS DS345 Synthesized Function Generator that provides the measurement signal is accurate up to 0.1%. Additionally, the noise in each measurement signal is less than 0.5%. Considering the accuracy of the electronics and possible noise-related errors, the measured voltages were shifted by 0.5% and compared to nominal values. The resulting difference in the distributions would amount to error bars that are smaller than the symbols used in Figure 5a.

CONCLUSIONS

The thermal conductivity of the near wall has been investigated using a multilayer analytical model to extract the thermal conductivity of the near-wall region and studying the porosity difference at the near wall as compared to the bulk utilizing micro-CT. It was found that there is a slightly smaller porosity value of 33.18% at 0.4 mm near wall compared to 33.31% in the bulk of the pebble bed. An analytical model was fitted to the experimental data with a two-parameter fit varying the thermal conductivity and diffusivity of the near-wall layer. The thermal conductivity was found to be 7.6 W m^{-1} K^{-1} at the near wall compared to the bulk values of 0.22 W m^{-1} K^{-1}. The decrease in porosity near the wall is not enough to account for this large difference in thermal properties. The temperature difference and discrepancies in thermal contact resistance were also called to the question; however, they would not contribute to the discrepancy in the thermal conductivity. However, it is clear that the resulting near-wall effective thermal conductivity closely emulates the thermal conductivity of a single pebble. It is speculated that in the near-wall regime, conduction through the single pebble dominates, while far away, the interfaces between pebbles scatter phonons, and the convection in the porous media offers a parallel heat transfer channel through air, leading to a decreased effective thermal conductivity. A sensitivity parameter study was also performed to validate the uniqueness of the solutions for each individual layer.

AUTHOR INFORMATION

Corresponding Author

David Estrada − *Micron School of Materials Science and Engineering, Boise State University, Boise, Idaho 83725, United States; Center for Advanced Energy Studies, Boise State University, Boise, Idaho 83725, United States; Idaho National Laboratory, Idaho Falls, Idaho 83415, United States;* orcid.org/0000-0001-5894-0773; Email: daveestrada@boisestate.edu

Authors

Katelyn Wada − *Micron School of Materials Science and Engineering, Boise State University, Boise, Idaho 83725, United States*

Josh Eixenberger − *Micron School of Materials Science and Engineering, Boise State University, Boise, Idaho 83725, United States; Center for Advanced Energy Studies and Department of Physics, Boise State University, Boise, Idaho 83725, United States;* orcid.org/0000-0002-9816-7268

Dallin Stout − *Department of Mechanical and Biomedical Engineering, Boise State University, Boise, Idaho 83725, United States*

Brian J. Jaques − *Micron School of Materials Science and Engineering, Boise State University, Boise, Idaho 83725, United States; Center for Advanced Energy Studies, Boise State University, Boise, Idaho 83725, United States; Idaho National Laboratory, Idaho Falls, Idaho 83415, United States*

Todd Otanicar − *Department of Mechanical and Biomedical Engineering, Boise State University, Boise, Idaho 83725, United States*

Complete contact information is available at: https://pubs.acs.org/10.1021/acsomega.3c08202

Notes

The authors declare no competing financial interest.

ACKNOWLEDGMENTS

This work was prepared as an account of the work sponsored by the U.S. Department of Energy, Office of Nuclear Energy Advanced Sensors and Instrumentation program under DOE Contract DE- AC07-05ID14517. Neither the U.S. government nor any agency thereof nor any of their employees makes any warranty, expressed or implied, or assumes any legal liability or responsibility for the accuracy, completeness, or usefulness of any information, apparatus, product, or process disclosed, or represents that its use would not infringe privately owned rights. References herein to any specific commercial product, process, or service by trade name, trademark, manufacturer, or otherwise do not necessarily constitute or imply its endorsement, recommendation, or favoring by the U.S. government or any agency thereof. The views and opinions of the authors expressed herein do not necessarily state or reflect those of the U.S. government or any agency thereof. Additionally, this material is based on work supported under a University Nuclear Leadership Program Graduate Fellowship through the Department of Energy, Office of Nuclear Energy. The authors, Dallin Stout and Todd Otanicar, would like to acknowledge partial support for this work from the U.S. Department of Energy Solar Energy Technologies Office under award number DE-EE0009375. The authors also acknowledge Nipun Goel for supporting SEM imaging in Figure 2.

https://doi.org/10.1021/acsomega.3c08202
ACS Omega 2024, 9, 1614−1619

REFERENCES

(1) Siegel, N.; Gross, M.; Ho, C.; Phan, T.; Yuan, J. Physical properties of solid particle thermal energy storage media for concentrating solar power applications. *Energy Procedia* **2014**, *49*, 1015−1023.

(2) Clifford, K. H.; Ambrosini, A. *Thermal Energy Storage Technologies*; DOE ESHB, 2020; Chapter 12.

(3) Hu, G.; Zhang, H.; Liu, Q. Design optimization on characteristics of packed-bed thermal energy storage system coupled with high temperature gas-cooled reactor pebble-bed module. *Energy Convers. Manag.* **2022**, *257*, 115434.

(4) Zhao, D. L.; Li, Y.; Dai, Y. J.; Wang, R. Z. Optimal study of a solar air heating system with pebble bed energy storage. *Energy Convers. Manag.* **2011**, *52*, 2392−2400.

(5) Hu, G.; O'Grady, D.; Zou, L.; Hu, R. Development of a Reference Model for Molten-Salt- Cooled Pebble-Bed Reactor Using SAM. *ANL/NSE*, 2020.

(6) Robert, Y.; Siaraferas, T.; Fratoni, M. Proof of concept for hyper-fidelity depletion of full-scale pebble bed reactors. *Ann. Nucl. Energy* **2023**, *183*, 109648.

(7) Rao, N. N.; Chaturvedi, V.; Li Puma, G. Novel pebble bed photocatalytic reactor for solar treatment of textile wastewater. *Chem. Eng. J.* **2012**, *184*, 90−97.

(8) Magnusson, J.; Memmott, M.; Munro, T. Review of thermophysical property methods applied to fueled and un-fueled molten salts. *Ann. Nucl. Energy* **2020**, *146*, 107608.

(9) Ramos, R.; Aresti, L.; Yiannoukos, L.; Tsiolakis, E.; Pekris, J.; Vieira, A.; Florides, G.; Christodoulides, P. Thermal and physical characteristics of soils in Cyprus for use in shallow geothermal energy applications. *Energy, Ecol. Environ.* **2019**, *4*, 300−309.

(10) Zhu, X.; Zhang, Q.; Wang, W.; Liu, Y. Study on the influencing factors of rock-soil thermophysical parameters in shallow geothermal energy. *J. Groundwater Sci. Eng.* **2015**, *3*, 256−267.

(11) Zou, L.; Hu, G.; O'Grady, D.; Hu, R. Explicit modeling of pebble temperature in the porous-media model for pebble-bed reactors. *Prog. Nucl. Energy* **2022**, *146*, 104175.

(12) Johnson, E.; Tarı, I.; Baker, D. A Monte Carlo method to solve for radiative effective thermal conductivity for particle beds of various solid fractions and emissivities. *J. Quant. Spectrosc. Radiat. Transf.* **2020**, *250*, 107014.

(13) Zavattoni, S.; Barbato, M.; Pedretti, A.; Zanganeh, G. CFD simulations of a pebble bed thermal energy storage system accounting for porosity variations effects. *Solar Paces*, 2011.

(14) Zou, L.; Hu, G.; O'Grady, D.; Hu, R. Explicit modeling of pebble temperature in the porous-media model for pebble-bed reactors. *Prog. Nucl. Energy* **2022**, *146*, 104175.

(15) Suikkanen, H.; Ritvanen, J.; Jalali, P.; Kyrki-Rajamäki, R. Discrete element modelling of pebble packing in pebble bed reactors. *Nucl. Eng. Des.* **2014**, *273*, 24−32.

(16) Abdulmohsin, R. S.; Al-Dahhan, M. H. Characteristics of convective heat transport in a packed pebble-bed reactor. *Nucl. Eng. Des.* **2015**, *284*, 143−152.

(17) Bu, S.; Wang, J.; Sun, W.; Ma, Z.; Zhang, L.; Pan, L. Numerical and experimental study of stagnant effective thermal conductivity of a graphite pebble bed with high solid to fluid thermal conductivity ratios. *Appl. Therm. Eng.* **2020**, *164*, 114511.

(18) Bu, S.; Li, Z.; Ma, Z.; Sun, W.; Zhang, L.; Chen, D. Numerical study of natural convection effects on effective thermal conductivity in a pebble bed. *Ann. Nucl. Energy* **2020**, *144*, 107524.

(19) De Beer, M.; Du Toit, C. G.; Rousseau, P. G. Experimental study of the effective thermal conductivity in the near-wall region of a packed pebble bed. *Nucl. Eng. Des.* **2018**, *339*, 253−268.

(20) Baumann, T.; Zunft, S. Properties of granular materials as heat transfer and storage medium in CSP application. *Sol. Energy Mater. Sol. Cells* **2015**, *143*, 38−47.

(21) Khan, M. I.; Asfand, F.; Al-Ghamdi, S. G. Progress in research and technological advancements of thermal energy storage systems for concentrated solar power. *J. Energy Storage* **2022**, *55*, 105860.

(22) Chung, K. M.; Zeng, J.; Adapa, S.; Feng, T.; Bagepalli, M.; Loutzenhiser, P.; Albrecht, K.; Ho, C.; Chen, R. Measurement and analysis of thermal conductivity of ceramic particle beds for solar thermal energy storage. *Sol. Energy Mater. Sol. Cells* **2021**, *230*, 111271.

(23) Jacob, R.; Sergeev, D.; Müller, M. Valorisation of waste materials for high temperature thermal storage: a review. *J. Energy Storage* **2022**, *47*, 103645.

(24) Wada, K.; Fleming, A.; Estrada, D. Novel Thermal Conductivity Measurement Technique Utilizing a Transient Multilayer Analytical Model of a Line Heat Source Probe for Extreme Environments. *Energy Technology 2023*; Springer, 2023.

(25) Wada, K.; Fleming, A.; Eixenberger, J.; Jaques, B. J.; Estrada, D. Transient multilayer analytical model of a line heat source probe for in-pile thermal conductivity measurements. *Int. J. Therm. Sci.* **2023**, *188*, 108241.

(26) Hollar, C.; Fleming, A.; Davis, K.; Budwig, R.; Jensen, C.; Estrada, D. A parametric study for in-pile use of the thermal conductivity needle probe using a transient, multilayered analytical model. *Int. J. Therm. Sci.* **2019**, *145*, 106028.

(27) Daw, J. E.; Rempe, J. L.; Knudson, D. L. Hot wire needle probe for in-reactor thermal conductivity measurement. *IEEE Sens J.* **2012**, *12*, 2554−2560.

(28) Nabil, M.; Khodadadi, J. M. Computational/analytical study of the transient hot wire-based thermal conductivity measurements near phase transition. *Int. J. Heat Mass Tran.* **2017**, *111*, 895−907.

(29) Rusconi, R.; Williams, W. C.; Buongiorno, J.; Piazza, R.; Hu, L. W. Numerical analysis of convective instabilities in a transient short-hot-wire setup for measurement of liquid thermal conductivity. *Int. J. Thermophys.* **2007**, *28*, 1131−1146.

(30) Rempe, J. L.; Knudson, D.; Daw, J.; Unruh, T.; Chase, B.; Palmer, J.; Condie, K.; Davis, K. *Enhanced in-Pile Instrumentation at the Advanced Test Reactor*; ANIMMA, 2011.

(31) Antoniadis, K. D.; Tertsinidou, G. J.; Assael, M. J.; Wakeham, W. A. Necessary Conditions for Accurate, Transient Hot-Wire Measurements of the Apparent Thermal Conductivity of Nanofluids are Seldom Satisfied. *Int. J. Thermophys.* **2016**, *37*, 78−22.

(32) Bhattacharya, S.; Nani, S.; Dasgupta, S.; De, S. Analytical solution of transient heat transfer with variable source for applications in nuclear reactors. *Int. Commun. Heat Mass Transfer* **2001**, *28*, 1005−1013.

(33) Chung, K. M.; Zeng, J.; Adapa, S.; Feng, T.; Bagepalli, M.; Loutzenhiser, P.; Albrecht, K.; Ho, C.; Chen, R. Measurement and analysis of thermal conductivity of ceramic particle beds for solar thermal energy storage. *Sol. Energy Mater. Sol. Cells* **2021**, *230*, 111271.

(34) Maillet, D.; Batsale, J.-C.; Andre', S.; Degiovanni, A. *Thermal Quadrupoles, Solving the Heat Equation through Integral Transforms*; John Wiley & Sons, LTD, 2000.

(35) Christen, C. E.; Gómez-Hernández, J.; Otanicar, T. P. Bimodal particle distributions with increased thermal conductivity for solid particles as heat transfer media and storage materials. *Int. J. Heat Mass Tran.* **2022**, *184*, 122250.

(36) Graczykowski, B.; El Sachat, A.; Reparaz, J.; Sledzinska, M.; Wagner, M.; Chavez-Angel, E.; Wu, Y.; Volz, S.; Wu, Y.; Alzina, F.; Sotomayor Torres, C. Thermal conductivity and air-mediated losses in periodic porous silicon membranes at high temperatures. *Nat. Commun.* **2017**, *8*, 415−416.

(37) Woodside, W. Calculation of the Thermal Conductivity of Porous Media. *Can. J. Phys.* **1958**, *36*, 815−823.

(38) Asakuma, Y.; Asada, M.; Kanazawa, Y.; Yamamoto, T. Thermal analysis with contact resistance of packed bed by a homogenization method. *Powder Technol.* **2016**, *291*, 46−51.

https://doi.org/10.1021/acsomega.3c08202
ACS Omega 2024, 9, 1614−1619